An Experimental Study on the Fatigue Response of 15-5 PH Stainless Steel Built by DMLS

D. Croccolo[1], M. De Agostinis[1], S. Fini[1], G. Olmi[1*], A. Vranic[2], S. Ciric-Kostic[2]
[1]Department of Industrial Engineering (DIN), University of Bologna, Bologna, Italy
[2]Faculty of Mechanical and Civil Engineering in Kraljevo, University of Kragujevac, Serbia

The present study is focused on the fatigue strength of 15-5 PH stainless steel parts built by DMLS. Four sets of specimens were manufactured, mechanically and thermally treated, and tested under rotating bending fatigue. The samples of the first two sets were built with their longitudinal axis perpendicular or parallel to the vertical stacking direction. In both cases, a 1mm allowance was uniformly distributed. The samples of the third and the fourth sets were similarly generated, with the same orientations. The samples of the last two sets were built with cylindrical shape and with 3mm allowance at gage. The results, processed also by analysis of variance tools, indicate that, considering the first two sets, the fatigue limit, approximately 39% of the ultimate strength, is almost independent of the build orientation. Conversely, the samples with incremented allowance, which required significant machining at gage, exhibit a much higher fatigue limit, very close to the commonly accepted reference value of one-half of the ultimate strength. This is quite an interesting result, as machining seems to be able to remove the process-induced irregularities, thus making it possible to achieve comparable properties to those of wrought material.

Keywords: Fatigue strength, Stainless steel, Additive manufacturing, Direct Metal Laser Sintering, Build orientation, Machining

1. INTRODUCTION

Nowadays, there is an increasing interest towards Additive Manufacturing (*AM*) techniques, as this technological process is potentially capable of producing even complexly shaped parts in a relatively short time [1]. In addition, the parts can be easily built, starting from a *CAD* model, which is automatically processed to determine the main manufacturing parameters and the required amount of material. The parts are built layer by layer in a similar manner to rapid prototyping of plastic materials: a high-power laser beam scans over a metallic powder bed and selectively melts the powder. The melted powder solidifies and forms a layer: upon the completion of each layer, powder is added, laser scanning is repeated and a subsequent layer is deposited [2-4]. The unused powder may be partly recycled for a further process. A possible drawback of *AM* techniques consists in the residual stresses that may be generated during part building. Therefore, suitably shaped supports are usually applied to safely attach the built part to a rigid base-plate, thus preventing its movements through the powder bed or distortions induced by the residual stress field [2]. Direct Metal Laser Sintering (*DMLS*) by *EOS* and Selective Laser Melting (*SLM*) by MTT Technologies Group can be mentioned among the most important *AM* processes for metals [4].

The aforementioned base-plate is usually placed on a horizontal plane, and the parts are generated along a vertical stacking direction. A number of studies, involving different materials and *AM* processes have been focused on the possible effect of the build direction on the mechanical static and fatigue responses of the manufactured parts. Some researchers investigated a possible influence of the angle between the main axis of inertia (namely, the longitudinal axis of the specimen) and the stacking direction on the part strength. Intensive studies were performed on selective laser melted Ti6-Al-4V samples. The results indicated that the build orientation may significantly affect the fatigue response, in particular the endurance strength in the finite life domain. A higher life for the same load entity was retrieved for the build orientation where the layer plane is parallel to the loading axis [5]. A similar effect was also observed on fracture toughness [6]. The possible effect of the build direction on the fatigue response, considering both the fatigue limit and the fatigue strength in the finite life domain was also the topic of a previous study by the same authors. This research involved MS1 Maraging steel parts, built, considering three different orientations, with post-manufacture mechanical and heat treatments. An extended experimental campaign led to the result that the fatigue response is not significantly affected by the build direction, since, for Maraging steels, post-manufacture treatments have a great role at removing sources of anisotropy [7].

Further research in the literature was focused on the mechanical behaviour 15-5 PH stainless steel parts. This type of steel is commonly used in applications such as aircraft components, or for parts under high pressure or working in harsh corrosive environments, including valves, shafts, fasteners, fittings and gears [2, 8]. A lack of studies on the effect of the build direction on the fatigue properties of this steel can be pointed out. In particular, the research in [2] was focused on the build orientation effect on the static response only. Experimental results indicated that the response is enhanced, when the load direction acts along the layer plane, but the fatigue properties for different build directions were not investigated. Other studies are documented in [9-10], but are more oriented to the effects on technological issues like machinability, rather than to the outcomes on the fatigue strength.

*Corresponding author: Giorgio Olmi, Department of Industrial Engineering (DIN), University of Bologna, Viale del Risorgimento 2, 40136 Bologna, Italy, e-mail: giorgio.olmi@unibo.it

The subject of this paper consists in an experimental study on the fatigue response of 15-5 PH stainless steel parts fabricated by the *DMLS* process. Two factors were considered: the build direction and the fabrication procedure. In particular, two different build orientations were considered, with the main axis of inertia of the parts being aligned to the load direction or perpendicular to it. Regarding the fabrication procedure, the effect of allowance and subsequent machining was studied: in one case, a conventional 1mm allowance was considered, whereas, in the second one, a larger allowance was adopted with the consequent need of machining to the core of the part. Issues of novelty arise from the lack of studies dealing with fatigue on this steel. Furthermore, the general absence of investigations on the effect of allowance on the properties of *AM* processed parts of any material must be emphasized.

2. MATERIALS AND METHODS

The experimental campaign was performed under rotating bending, following the ISO1143 [11] Standard. Specimens were designed accordingly with reference to the cylindrical smooth geometry (with uniform cross section at gauge). The smallest dimension suggested by the standard, 6mm diameter at gauge was chosen as a good compromise between standard requirements and the need of reducing production costs. A drawing of the specimen is shown in Fig. 1, with indication of all its dimensions and tolerances. The chemical composition of 15-5 PH stainless steel (by EOSGmbH – Electro Optical Systems, Krailling/Munich, Germany) is provided in Table 1 [12].

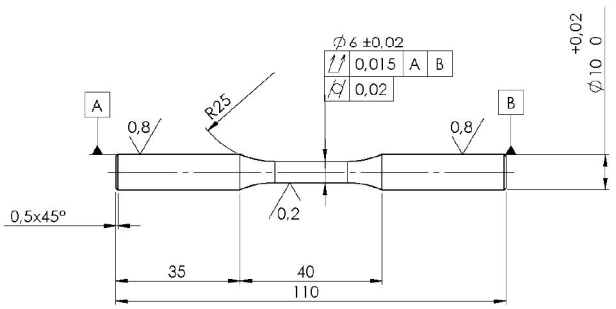

Figure 1: Specimen with 6 mm diameter at gage in agreement with ISO 1143 Standard [11]

Table 1: Chemical composition of 15-5 PH Stainless Steel by EOS

Cr [%]	Ni [%]	Cu [%]	Mn [%]	Si [%]	Mo [%]	Nb [%]	C [%]	Fe [%]
14-15.5	3.5-5.5	2.5-4.5	≤ 1	≤ 1	≤ 0.5	0.15-0.45	≤ 0.07	Balance

The specimens were manufactured by EOSINT M280 system (EOS GmbH - Electro Optical Systems, Krailling/Munich, Germany), equipped with Ytterbium fibre laser with 200W power and emitting 0.2032mm thickness and 1064nm wavelength infrared light beam. The process takes place in an inert environment and the scanning speed may range up to 7000 mm/s. The layer thickness was set to 20 μm. A parallel scan strategy with alternating scan direction was adopted: for the subsequent layers the scanning direction was rotated to 70°, in order to prevent or reduce in-plane property variations. Some examples of the scanning patterns are shown in Fig. 2, where arrows indicate the different scan directions at different stages of production and on different layers. A contour line was finally scanned, in order to complete the part shaping and to make its external surface as smoother as possible [13]. The machine features a working space with 250 × 250mm dimensions on the horizontal plane and a maximum height of 325mm.

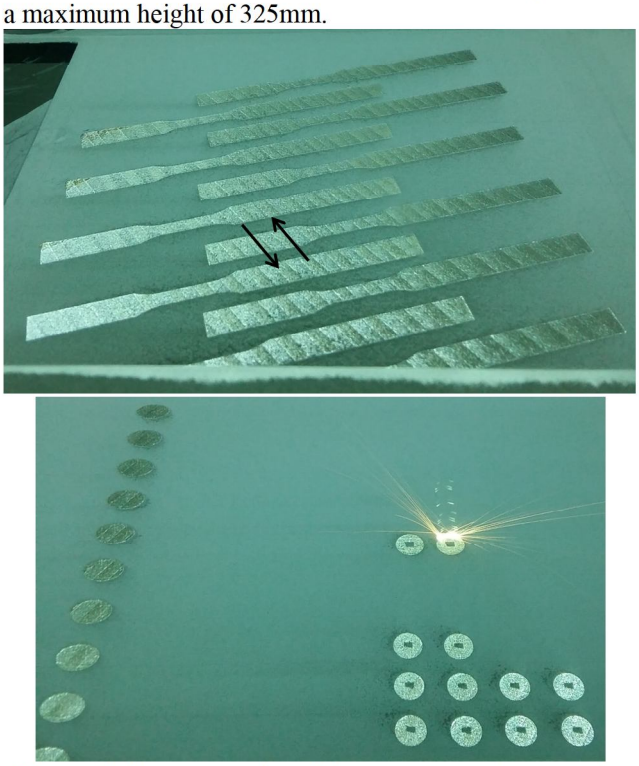

Figure 2: Some examples of the scanning patterns as the specimens are being built (arrows indicate the scan directions)

All the specimens underwent surface cleaning by micro-shot-peening: this treatment is usually performed in order to close the pores that may be induced by laser sintering. Afterwards, H900 heat treatment was performed [2, 12]: it consists in gradual heating in oven from room temperature to 482°C in 1 hour time, afterwards this temperature is kept constant for 2 hours. The parts are finally taken out of the oven and cooled in fresh air. This treatment, which is particularly effective at reducing the residual stresses, thus enhancing the fatigue response of the built parts, was performed maintaining the samples attached to their supports to prevent them from bending. Finally, the specimens underwent machining and refining by grinding with the aim of achieving the surface roughness requested by the ISO 1143 Standard [11] and of improving the fatigue performance.

Four specimen sets were manufactured: those of types #1 and #3 were built while lying horizontally on the base plate, therefore the angle between their longitudinal axis and the vertical stacking direction was 90°. Whereas, those of types #2 and #4 were built along the vertical direction: in this condition, the angle between their main axis of inertia and the stacking direction was 0°. The difference between the samples of sets #1 and #3 is that the first ones were produced with the same shape as shown in Fig. 1 with a 1mm allowance both at the gage (diameter increased from 6 to 8 mm) and at the heads (diameter increased from 10 to 12 mm). The samples were then machined to meet the drawing specifications, regarding

dimensional and geometrical tolerances and roughness. Conversely, the samples of set #3 were built with a cylindrical shape with 12 mm diameter over their entire length. It means that the allowance was 1mm at the heads and 3mm at the specimen gage. These samples were also reworked to meet the same specifications of the drawing in Fig. 1. The same difference applies also to sets #2 (built with uniform allowance and reduced section at gage) and #4 (built with cylindrical layout). Each set was composed by 7 to 10 samples, considering that some samples were unfortunately damaged during manufacturing. Some stages of production, with reference to the aforementioned sample sets, are shown in Fig. 3.

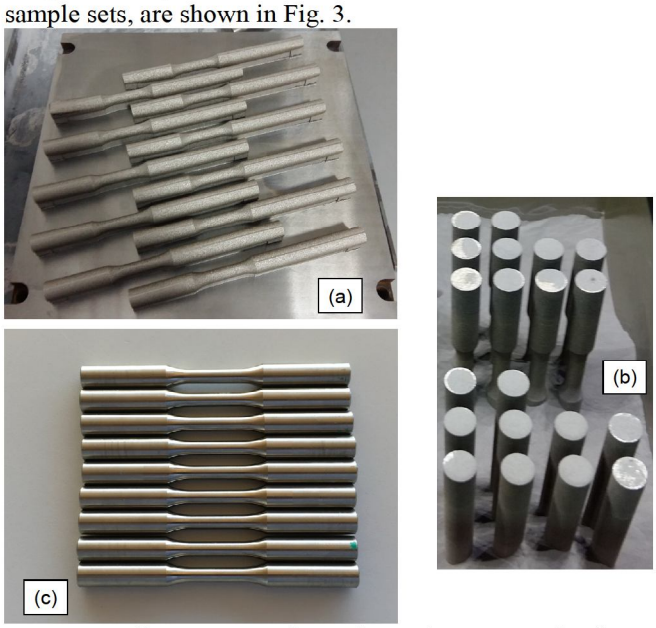

Figure 3: Some stages of sample production: (a) Set #1 samples just after DMLS manufacturing and before the heat treatment, (b) Sets #2 and #4 samples during residual powder removal with internal gage (top) and cylindrical shape (bottom), (c) Set #3 samples after machining and finishing, just before the beginning of the fatigue campaign

The fatigue campaign made it possible to obtain the *S-N* curves and the fatigue limits (*FL*s). A staircase method was applied to determine the *FL*: for this purpose, the series of failure and not-failure events was processed by the Dixon method [14-17]. A life duration of 107 cycles was set as run-out, based on the few available data on the fatigue response of sintered 15-5 PH stainless steel [2]. The Dixon method is an abbreviated staircase method that makes it possible to estimate *FL* even from a short series of nominal trials at staircase (four to six in this work). The estimation of the standard deviation makes also possible to provide an estimation of the uncertainty of the *FL* and to determine a confidence band to be applied to it. The data in the finite life domain were processed according to the Standard ISO 12107 [18]: the stress and life were linearly interpolated in logarithmic coordinates. The lower and upper limits of the *S-N* curve were been determined, based on the standard deviation of the logarithm of the fatigue life, and considering, respectively, probabilities of failure of 10% and 90% and a 90% confidence level.

3. EXPERIMENTAL PROCEDURE

All the samples were initially measured, in order to check the accomplishment of drawing requirements from the points of view of dimensions and roughness. For this purpose, a micrometre screw gauge, a digital calliper (both with the resolution of 0.01mm) and a portable surface roughness tester (with the resolution of 0.01 μm, Handysurf E-30A; Carl Zeiss AG, Oberkochen, Germany) were used. The heads at both ends and the sample gauges were measured at 90° angled points with 4 replications. Similar measurements were performed at specimen gages with 6 replications. The averaged values are collected in Tables 2-5, referred to the left-side head of the four sample sets. Regarding roughness, it has also been measured, considering 90° angled points around full diameters at both specimen heads with 8 replications. Similar measurements were then carried out at the gages after sample breakage. The averaged values are included as well in the same Tables. All the yields are generally well consistent with the requirements in ISO 1143 [11] and with drawing specifications. The samples were also checked for hardness: *HRC* Rockwell hardness was determined on all the samples with three replications. The average values, ranging from 42 to 43.5 *HRC* confirm an Ultimate Tensile Strength (*UTS*) from 1325 to 1375 MPa, which is in the order of that indicated in [12, 19-20] of 1310 MPa.

Table 2: Measurement outcomes for the sample type #1

	Gauge diameter			Head diameter		
Specimen ID	Mean [mm]	St dev. [mm]	Roughness [μm]	Mean [mm]	St dev. [mm]	Roughness [μm]
1.1	6.01	0.064	0.190	10.04	0.014	0.44
1.2	5.89	0.106	0.200	9.93	0.055	0.52
1.3	6.09	0.064	0.296	10.06	0.005	0.27
1.4	6.06	0.022	X	10.06	0.010	0.39
1.5	6.05	0.029	0.289	10.03	0.012	0.59
1.6	6.07	0.031	0.128	10.04	0.021	0.60
1.7	6.00	0.039	0.178	9.99	0.020	0.17

Table 3: Measurement outcomes for the sample type #2

	Gauge diameter			Head diameter		
Specimen ID	Mean [mm]	St dev. [mm]	Roughness [μm]	Mean [mm]	St dev. [mm]	Roughness [μm]
2.1	6.03	0.035	0.400	10.01	0.005	0.38
2.2	6.01	0.029	0.323	10.01	0.002	0.30
2.3	6.02	0.036	0.413	10.01	0.004	0.31
2.4	5.98	0.044	0.246	10.01	0.005	0.41
2.5	6.02	0.027	0.425	10.01	0.003	0.35
2.6	6.00	0.026	0.338	10.00	0.002	0.35
2.7	6.01	0.035	X	10.01	0.002	0.37
2.8	6.02	0.036	0.340	10.00	0.003	0.35
2.9	6.01	0.025	0.370	10.00	0.003	0.36
2.10	6.00	0.038	0.308	10.00	0.010	0.44

Table 4: Measurement outcomes for the sample type #3

	Gauge diameter			Head diameter		
Specimen ID	Mean [mm]	St dev. [mm]	Roughness [μm]	Mean [mm]	St dev. [mm]	Roughness [μm]
3.1	6.01	0.014	0.270	10.02	0.002	0.64
3.2	6.01	0.016	0.340	10.02	0.005	0.48
3.3	6.01	0.011	X	10.01	0.003	0.71
3.4	6.00	0.009	0.260	10.02	0.009	0.65
3.5	6.01	0.010	X	10.02	0.003	0.50
3.6	6.00	0.014	0.440	10.02	0.005	0.59
3.7	6.01	0.008	0.250	10.02	0.003	0.63
3.8	6.01	0.009	0.400	10.02	0.003	0.64
3.9	6.00	0.012	0.350	10.02	0.004	0.63

Table 5: Measurement outcomes for the sample type #4

	Gauge diameter			Head diameter		
Specimen ID	Mean [mm]	St dev. [mm]	Roughness [μm]	Mean [mm]	St dev. [mm]	Roughness [μm]
4.1	6.03	0.041	0.300	10.00	0.002	0.22
4.2	6.00	0.019	0.369	10.00	0.003	0.28
4.3	6.00	0.028	X	10.00	0.003	0.23
4.4	6.01	0.040	0.363	10.00	0.003	0.30
4.5	6.00	0.036	X	10.00	0.002	0.32
4.6	6.01	0.040	0.398	10.00	0.003	0.31
4.7	6.01	0.026	X	10.00	0.003	0.25
4.8	6.02	0.032	0.328	10.00	0.003	0.27
4.9	6.00	0.019	0.478	10.00	0.003	0.24
4.10	6.00	0.018	0.280	10.00	0.002	0.23

The specimens were tested under rotating bending fatigue by a rotary bending testing machine, where the specimen is loaded in the four-point bending configuration, so that bending moment keeps constant over the entire sample length, and in particular at its gage [14]. The sample was pinched at its ends by a pressure of approximately 70 MPa [21-22]. All the tests were conducted under fully reversed bending load (stress ratio R =-1) at the frequency f of 60 Hz. At the end of the experimental campaigns, some samples were cut and resin embedded. In particular, transverse sections of the gages and longitudinal sections of the heads were considered. Micrographic analyses were performed both at the gages and at the ends, following chemical attacks according to this recipe. 20 cc of Glycerol ($C_3H_8O_3$) and 10 cc Nitric Acid (HNO_3) were mixed together and the same was done with 20 cc of Chloridric Acid (HCl) and 10 cc of Hydrogen peroxide (H_2O_2). These two mixtures were finally 50%-50% mixed together.

4. RESULTS

The results of the fatigue tests for type #1 specimens (horizontally built, with 1mm allowance) are collected in Table 6: in particular, sample identifier, the load level in terms of the applied force and of the nominal stress at gage, the observed life and the test outcome are reported.

Table 6: Data retrieved from the tests on the sample type #1

Specimen ID	Load [N]	Stress [MPa]	Life [N]	Failure
1.1	127.2	420	---	N
1.2	166.6	550	144,726	Y
1.3	158.8	524	167,829	Y
1.4	151.5	500	---	N
1.5	151.5	500	728,708	Y
1.6	143.9	475	8,423,284	Y
1.7	197.2	651	47,315	Y

Table 7: Data retrieved from the tests on the sample type #2

Specimen ID	Load [N]	Stress [MPa]	Life [N]	Failure
2.1	197.2	651	4,834,809	Y
2.2	215.4	711	1,871,476	Y
2.3	178.7	590	108,926	Y
2.4	178.7	590	68,686	Y
2.5	142.8	470	---	N
2.6	169.6	560	43,729	Y
2.7	160.6	530	---	N
2.8	169.6	560	2,807,208	Y
2.9	160.6	530	2,564,861	Y
2.10	151.5	500	5,047,111	Y

Table 8: Data retrieved from the tests on the sample type #3

Specimen ID	Load [N]	Stress [MPa]	Life [N]	Failure
3.1	206.0	680	---	N
3.2	215.4	711	3,274,162	Y
3.3	206.0	680	---	N
3.4	215.4	711	8,364,965	Y
3.5	206.0	680	---	N
3.6	242.4	800	183,582	Y
3.7	233.3	770	368,551	Y
3.8	224.2	740	297,241	Y
3.9	224.2	740	2,850,771	Y

Table 9: Data retrieved from the tests on the sample type #4

Specimen ID	Load [N]	Stress [MPa]	Life [N]	Failure
4.1	196.9	650	6,082,766	Y
4.2	215.4	711	7,366,205	Y
4.3	242.4	800	532,725	Y (NOT VALID)
4.4	178.7	590	---	N
4.5	187.8	620	1,256,019	Y (NOT VALID)
4.6	187.8	620	8,932,232	Y
4.7	178.7	590	---	N
4.8	187.8	620	6,397,216	Y
4.9	242.4	800	260,944	Y
4.10	233.3	770	503,334	Y

The results of sets #2 (vertically built, with uniform allowance), #3 (horizontally built, with greater allowance at gage) and #4 (vertically built, with greater allowance at gage) are respectively reported in Tables 7-9, where the same data are present. A not failure outcome indicates that the trial was stopped upon run-out without breakage occurrence. In the case of failure, it was of course checked that specimen separation had occurred at gage. Afterwards, the fracture surfaces were observed to make sure that a fatigue initiation and propagation mechanism was actually responsible of the observed failure. Most failures regularly occurred at gage, but in two cases, for the same sample set (Set #4), unusual and unexpected failures at specimen heads were observed. One of these failures is depicted in Fig. 4. It must be remarked that this outcome is not completely new, as it had also been observed (again in two cases) in the previous research regarding Maraging steels. In that study, an analysis by dye penetrants had indicated the presence of some spots of unconformable roughness, which were likely to have triggered the crack in combination with the clamping

pressure. In the present study, the roughness at sample ends was carefully checked by multiple measurements and was found to be consistent with specifications. The analysis was therefore deepened by micrographic analyses, as described in the previous Section.

Figure 4: Unexpected failure at sample head

The samples that were involved in the aforementioned outcome were of course discarded for further processing regarding the fatigue response. The final outcomes of these two trials are therefore tagged as NOT VALID in Table 9. The other results were anyway sufficient to determine both the sloping part of the S-N curve and the fatigue limit.

5. DISCUSSION

The results reported in the previous Section were initially processed, in order to determine the fatigue curves in the finite life domain. The *S-N* curves, retrieved as linear regressions in double logarithmic scale, are plotted in the graphs in Fig.s 6-9 for sets #1 to #4 respectively. The corresponding equations that yield the expected life as a function of the actual stress level are included in the figures. The related maximum likelihood bands at the 90% confidence level and the experimental data are also plotted in the same diagrams, following the recommendations of [18]. The experimental results can be generally well fitted along a straight line with a linear correlation coefficient (R^2) up to 0.8.

The slopes of the interpolating lines were also determined during the regression procedure. The angle between the *S-N* line and the vertical axis is 86° for set #1, 88° for set #2, 88° for set #3 and 85° for set #4. The resulting inclination can be compared to those of the *S-N* curves determined for Maraging Steel MS1: considering Ref. [7] the angles of the determined curves were ranging between 75° and 80°. The generally higher angle retrieved for stainless steel indicates that its *S-N* curves have a less steep trend, where small variations of the state of load may correspond to huge variations of the fatigue life, from the order of 10^5 to almost 10^7 cycles. A great role seems to be due to the level of roughness: as documented by the data in Tables 2-5, related values were quite low in this study, ranging from 0.2 to 0.3μm as an average. The experimentations reported in [19-20] were performed on samples of the same material and with comparable roughness and led to a nearly horizontal curve, with a similar slope. Conversely, the experimentations in [2], involving the same stainless steel produced by *SLM*, were performed on samples with a 10-time higher roughness and led to a much lower fatigue resistance with a particularly sharp drop of the curve for increasing life (corresponding to a much lower angle).

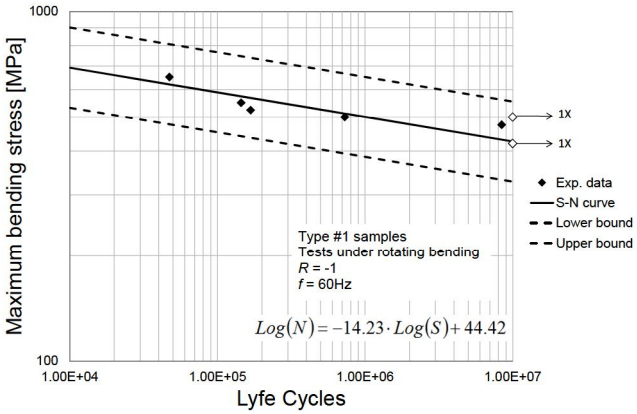

Figure 5: S-N curve for type #1 specimens (arrows indicate run-outs)

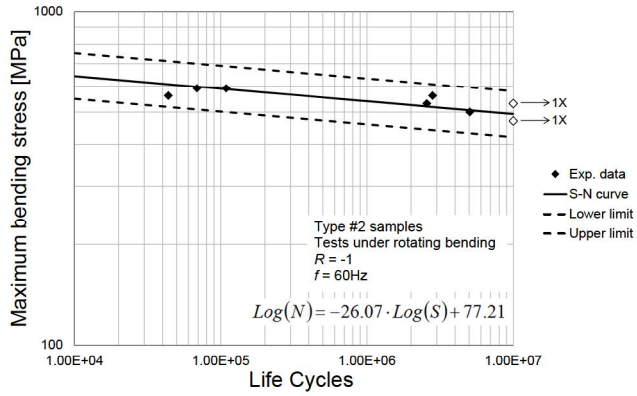

Figure 6: S-N curve for type #2 specimens (arrows indicate run-outs)

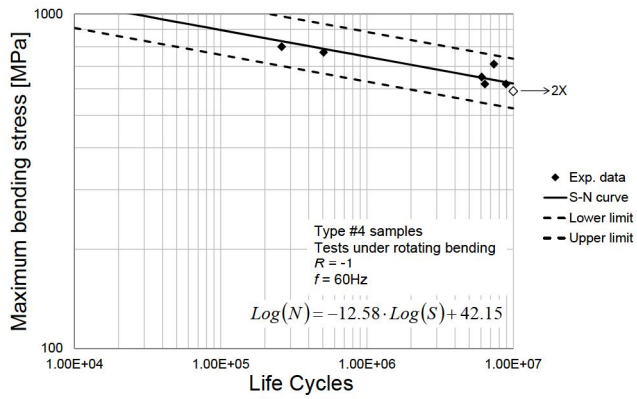

Figure 7: S-N curve for type #3 specimens (arrows indicate run-outs)

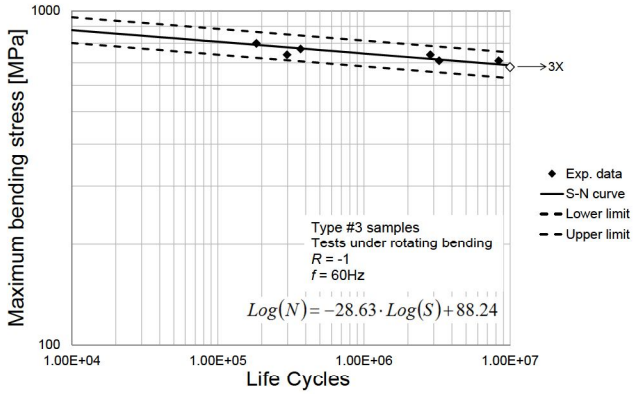

Figure 8: S-N curve for type #4 specimens (arrows indicate run-outs)

The results of the trials at staircase were processed by the Dixon method and led to the estimation of the *FL*s collected in the bar graph in Fig. 10, along with related confidence bands. The limit for the sample type #1 was estimated as 480 MPa, a well comparable value to that for type #2, 507 MPa. The other limits were conversely significantly higher: 701MPa for type #3 and 605MPa for the fourth sample set.

It is interesting to compare the determined *FL*s to the *UTS* strength of the material according to [12, 19-20], considering that a commonly accepted ratio (*FL*/*UTS*) is approximately 50% for metallic materials [23]. The *FL*s for horizontally and vertically built samples with 1mm allowance are quite close each other and correspond to 37% and 39% of the *UTS*. This isotropic behavior is consistent to that reported in [7] for Maraging steels. Moreover, the determined ratios to *UTS* are lower than 50%, but about ten points higher than the same ratio determined for Maraging steel. It indicates that, on one hand the *DMLS* processed parts have a lower fatigue limit than expected, but that this detrimental effect is less significant for 15-5 Stainless steel rather than for Maraging steel.

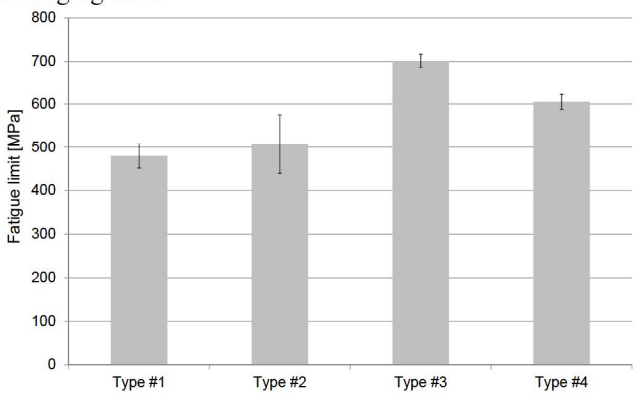

Figure 9: Bar graph summarizing the fatigue limits for the four sample types along with their confidence bands

Regarding the *FL*s for sets #3 and #4, ratios to *UTS* are respectively 54% and 46%. This outcome indicates that a post-manufacturc machining up to thc matcrial corc seems to have a beneficial effect on the fatigue response. In particular, the post-manufacture machining seems to be able to remove the irregularities at the surface layers, where, as remarked in the Materials and Methods Section, contour lines are scanned to complete the part shaping. These irregularities may be able to trigger fatigue cracks and may therefore be responsible of the aforementioned lower fatigue response of *DMLS* (and generally *AM*) processed parts. As a consequence, the ratio to *UTS* is significantly increased up to the reference value of 50%. Moreover, the response is better, when the load direction acts on the layer plane, which is consistent to the results in [5-6] for Maraging steels and in [2] for the same steel under static load.

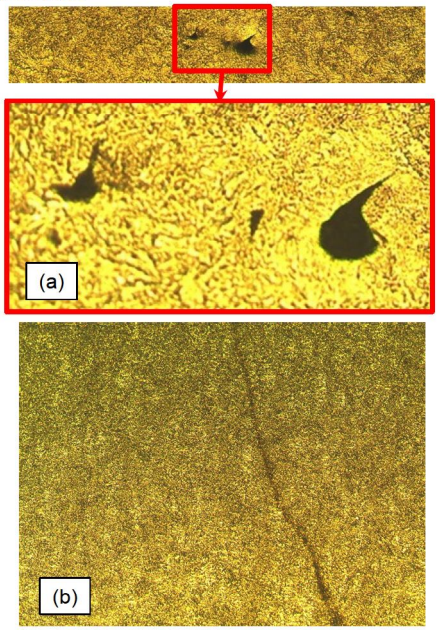

Figure 10: (a) Example of a void; (b) transverse crack detected at specimen head

Finally, some micrographic and fractographic analyses were performed on the samples, to check the material structure and to investigate the possible reasons for the unexpected failures at heads. It can be remarked that some voids were observed: an example is shown in Fig. 10 (a). These voids are likely to have triggered most of these irregular failures, acting in combination with the clamping pressure. In addition, it is interesting to observe that a transverse crack was observed at the head of a specimen of Set #4 that had regularly broken down at the gage. It may indicate that another crack was propagating at the head, but that separation at the gage occurred earlier.

The visual observation of the regular cracks at gage by stereo and optical microspores indicated that pores with 30-40μm diameter just beneath the surface (at about 80μm depth) were responsible for the initiation of most cracks. An example is shown in Fig. 11.

Finally, some micrographies were devoted to the observation of the microstructure generated by the building process: the picture in Fig. 12 (a) was taken along the build plane: it can be observed that laser scans on contiguous planes are well visible and the related angle (highlighted) is consistent with the process setting. A micrography along a perpendicular plane (parallel to the vertical stacking direction) is finally depicted in Fig. 12 (b), where the build direction is also indicated. These outcomes indicate that the *AM* induced structure is still well visible, even after the recommended heat treatments.

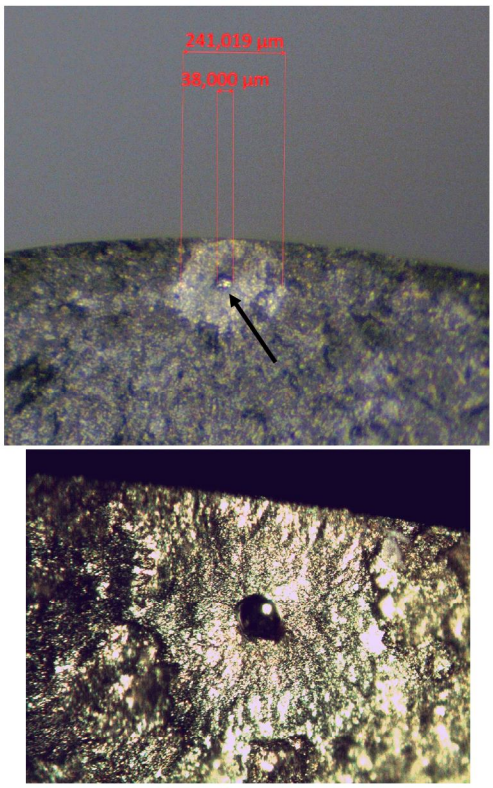

Figure 11: Example of a pore that triggered a crack

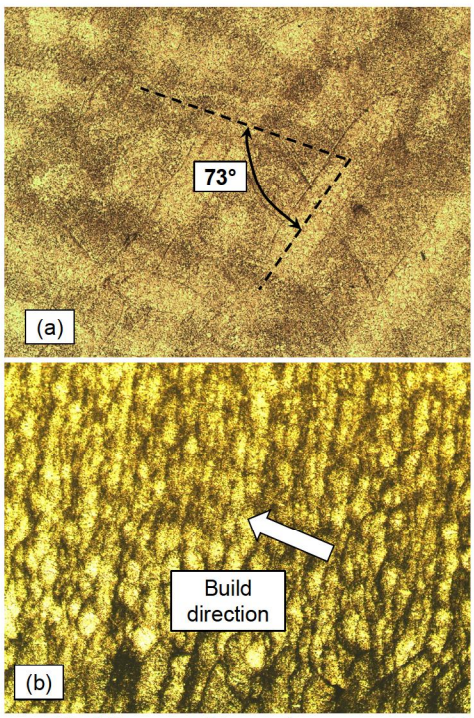

Figure 12: Micrographic analyses on unmachined horizontally built samples: (a) laser scans on the build plane (contiguous planes are visible, relative angle highlighted), (b) layers along the stacking direction

6. CONCLUSIONS

This study aims at defining the fatigue strength of 15-5 PH Stainless Steel manufactured by direct selective laser sintering (*DMLS*) machine. Literature survey indicated that Additive Manufacturing (*AM*) techniques, such as *DMLS* or Selective Laser Melting are highly effective at producing even complicated parts. Moreover, there is a lack of data concerning the fatigue response of *AM* processed parts of the aforementioned stainless steel. Four sample sets were manufactured: horizontally and vertically built with uniform allowance and with an incremented allowance at specimen gage (manufactured as cylindrical parts). This experiment can therefore be regarded as a two-factor plan with two levels (2^2). The results indicate that the fatigue curves have a high inclination with respect to the vertical axis and that the fatigue limits of horizontally and vertically built samples with uniform allowance are almost the same. The ratio of the fatigue limits to the ultimate tensile strength is approximately 38%. Conversely, when considering samples with higher allowance, which required the removal of a remarkable amount of material at gage, the fatigue limit is averagely one-half of the ultimate strength. Machining up to the material core seems to be able remove the additive process induced irregularities at the external layers that reduce the fatigue strength of *AM* processed parts. Moreover, the limit was higher for samples where the layer planes are parallel to the load direction. Afterwards, fractographic and micrographic analyses made it possible to provide explanations to the observed outcomes, and to check the microstructure resulting from the additive process.

ACKNOWLEDGEMENTS

The research presented in this paper has received funding from the European Union's Horizon 2020 research and innovation programme under the Marie Skłodowska-Curie grant agreement No. 734455.

REFERENCES

[1] F. Abe, K. Osakada, M. Shiomi, K. Uematsu and M. Matsumoto, "The manufacturing of hard tools from metallic powders by selective laser melting", Journal of Materials Processing Technology, Vol. 111, pp. 210-213, (2001)

[2] H.K. Rafi, T.L. Starr and B.E. Stucker, "A comparison of the tensile, fatigue, and fracture behaviour of Ti–6Al–4V and 15-5 PH stainless steel parts made by selective laser melting", The International Journal of Advanced Manufacturing Technology, Vol. 69, pp. 1299-1309 (2013)

[3] E. Santos, S. Masanari, K. Osakada and T. Laoui, "Rapid manufacturing of metal components by laser forming", International Journal of Machine Tools and Manufacture, Vol. 46, pp. 1459-1468 (2006)

[4] E. Herderick, "Additive Manufacturing of Metals: A Review", Proceedings of "Materials Science and Technology (MS&T)", October 16-20, 2011, Columbus, Ohio, (2011)

[5] P. Edwards and M. Ramulu, "Fatigue performance evaluation of selective laser melted Ti-6Al-4 V", Materials Science and Engineering A, Vol. 598, pp. 327-337, (2014)

[6] P. Edwards and M. Ramulu, "Effect of build direction on the fracture toughness and fatigue crack growth in selective laser melted Ti-6Al-4V", Fatigue & Fracture of Engineering Materials & Structures, Vol. 38, pp. 1228-1236 (2015)

[7] D. Croccolo, M. De Agostinis, S. Fini, G. Olmi, A. Vranic and S. Ciric-Kostic, "Influence of the build

orientation on the fatigue strength of EOS maraging steel produced by additive metal machine", Fatigue & Fracture of Engineering Materials & Structures, Vol. 39, pp. 637-647, (2016)

[8] M. Abdelshehid, K. Mahmodieh, K. Mori, L. Chen, P. Stoyanov, D. Davlantes, J. Foyos, J. Ogren, R. Clark Jr. and O.S. Es-Said, "On the correlation between fracture toughness and precipitation hardening heat treatments in 15-5PH Stainless Steel", Engineering Failure Analysis, Vol. 14, pp. 626-631, (2007)

[9] K. Ozbaysal and O.T. Inal, "Age-hardening kinetics and microstructure of PH 15-5 stainless steel after laser melting and solution treating", Journal of Materials Science, Vol. 29, pp. 1471-1480, (1994)

[10] D. Palanisamy, P. Senthil and V. Senthilkumar, "The effect of aging on machinability of 15Cr–5Ni precipitation hardened stainless steel", Archives of Civil and Mechanical Engineering, Vol. 16, pp. 53-63, (2016)

[11] International Organization for Standardization ISO 1143:2010, "Standard - Metallic materials – Rotating bar bending fatigue testing", International Organization for Standardization (ISO), Geneva, Switzerland, (2010)

[12] http://www.eos.info/material-m

[13] D. Croccolo, M. De Agostinis and G. Olmi, "Experimental characterization and analytical modelling of the mechanical behaviour of fused deposition processed parts made of ABS-M30", Computational Materials Science, Vol. 79, pp. 506-518, (2013)

[14] G. Olmi and A. Freddi, "A new method for modelling the support effect under rotating bending fatigue: Application to Ti-6Al-4V alloy, with and without shot peening", Fatigue and Fracture of Engineering Materials and Structures, Vol. 36 (10), pp. 981-993, (2013)

[15] W.J. Dixon and F. Massey Jr., "Introduction to Statistical Analysis", McGraw-Hill, New York, United States, (1983)

[16] G. Olmi, M. Comandini and A. Freddi, "Fatigue on shot-peened gears: Experimentation, simulation and sensitivity analyses", Strain, Vol. 46 (4), pp. 382-395 (2010).

[17] B. Van Hooreweder, D. Moens, R. Boonen and P. Sas, "The critical distance theory for fatigue analysis of notched aluminium specimens subjected to repeated bending", Fatigue and Fracture of Engineering Materials and Structures, Vol. 35, pp. 878-884 (2012)

[18] International Organization for Standardization ISO 12107:2003, "Metallic Materials – Fatigue Testing – Statistical Planning and Analysis of Data", International Organization for Standardization (ISO), Geneva, Switzerland, (2003)

[19] ASM International, "ASM Handbook", Vol. 1, Materials Park, Ohio, (2016)

[20] ASM International, "ASM Handbook", Vol. 2, Materials Park, Ohio (2016)

[21] D. Croccolo, M. De Agostinis and G. Olmi, "Fatigue life characterisation of interference fitted joints", Proceedings 2013 ASME International Mechanical Engineering Congress and Exposition", in Proc. IMECE 2013, San Diego, CA, United States, Vol. 2B, V02BT02A015 (10 pages), (2013)

[22] D. Croccolo, M. De Agostinis, S. Fini, A. Morri and G. Olmi G, "Analysis of the Influence of Fretting on the Fatigue Life of Interference Fitted Joints", Proceedings ASME - American Society of Mechanical Engineers, Montreal, Canada, 14-20, November, 2014, Vol. 2B: Advanced Manufacturing, pp. 1-10, 2014.

[23] G. Niemann, H. Winter, B.R. Hohn, "Maschinenelemente", Springer-Verlag, Berlin, Germany (2005)